Title

Using soft x-ray absorption spectroscopy to characterize electrode/electrolyte interfaces in-situ and operando

Authors

Ye, Yifan
Wu, Cheng Hao
Zhang, Liang
et al.

Publication Date

2017-11-01

DOI

10.1016/j.elspec.2017.05.002

Peer reviewed

Journal of Electron Spectroscopy and Related Phenomena 221 (2017) 2–9

Contents lists available at ScienceDirect

Journal of Electron Spectroscopy and Related Phenomena

journal homepage: www.elsevier.com/locate/elspec

Using soft x-ray absorption spectroscopy to characterize electrode/electrolyte interfaces *in-situ* and *operando*

Yifan Ye[a,1], Cheng Hao Wu[a,1], Liang Zhang[a], Yi-Sheng Liu[a], Per-Anders Glans-Suzuki[a], Jinghua Guo[a,b,*]

[a] Advanced Light Source, Lawrence Berkeley National Laboratory, Berkeley, CA 94720, USA
[b] Department of Chemistry and Biochemistry, University of California, Santa Cruz, CA 95064, USA

ARTICLE INFO

Article history:
Received 31 December 2016
Accepted 1 May 2017
Available online 2 May 2017

Keywords:
Solid/liquid interface
Electrochemical double layer
Soft x-ray absorption spectroscopy
Liquid cell

ABSTRACT

The interfaces between electrode and electrolyte play a vital role in various electrochemical systems. However, the understanding of such embedded interfaces and interfacial processes is still limited partly because of the short of proper characterizations tools, especially *in-situ*/*operando* techniques. In the past decade, substantial effort has been devoted in the development of *in-situ*/*operando* techniques to investigate the solid/liquid interfaces. One successful approach is the combination of *in-situ* liquid cells and soft x-ray absorption spectroscopy (sXAS). In this review, we showcased several recent examples using such liquid-cell-based *in-situ*/*operando* sXAS method to study different aspects of the electrode/electrolyte interface under reaction conditions, including the adsorption and deposition of solute species on electrode surface, morphological and chemical changes of electrode surface, and potential-dependent orientations of interfacial solvent molecules. These examples demonstrated capability of such *in-situ*/*operando* sXAS techniques in providing element- and chemical-sensitive interfacial information. This *in-situ*/*operando* sXAS technique also opens the way to the investigation of various solid/liquid interfaces in other important heterogeneous reactions.

1. Motivation

The consumption of traditional fossil fuel has serious environmental impact on the global level, which has become more serious in recent years. Thus, there have been tremendous interests and demands to develop next-generation energy-generation and energy-storage technologies and devices that need to be efficient, low-cost, and environmentally friendly. Promising candidate technologies include photo-catalysis [1,2], photo-electrocatalysis [3], fuel cells [4], and various batteries [5–7], many of which are based on electrochemistry. To achieve optimum performance of these electrochemical devices, it is crucially important to first understand the mechanisms of relevant electrochemical reactions.

Classic electrochemistry theories, mostly continuum theories, suggested that electrode/electrolyte interface plays a vital role in various electrochemical systems [8–10]. During an electrochemical reaction, several elemental processes can take place at the electrode/electrolyte interface, such as selective adsorption of solvent and solvated ions on electrode surface, deposition and dissolution of solvated ions, charge transfer between electrodes and electrolytes, and ion intercalation into the electrodes, as schematically shown in Fig. 1 [11]. Therefore, the capability to characterize the physicochemical properties of the interfaces and to observe these interfacial processes is extremely beneficial for the understanding of the reaction mechanism of relevant electrochemical reactions. However, the unique boundary conditions imposed on the materials at the solid/liquid interface make their properties and behaviors drastically different from that of their bulk counterparts or even the surfaces in vacuum [12]. Moreover, such imbedded interface is rather challenging to characterize, because many surface/interface-sensitive characterization techniques require high vacuum, for instance, x-ray photoelectron spectroscopy (XPS) [13–15], electron energy loss spectroscopy (EELS) [13], x-ray absorption/emission spectroscopy (XAS/XES) [16,17], scanning tunneling microscopy (STM) [18], scanning transmission x-ray microscopy (STXM) [19], and (scanning) transmission electron microscopy (TEM/STEM) [16]. Most previous investigations of the solid/liquid interface using these conventional surface science characterization techniques

* Corresponding author at: Advanced Light Source, Lawrence Berkeley National Laboratory, Berkeley, CA 94720, USA; Department of Chemistry and Biochemistry, University of California, Santa Cruz, CA 95064, USA.
E-mail address: jguo@lbl.gov (J. Guo).
[1] These authors contributed equally.

http://dx.doi.org/10.1016/j.elspec.2017.05.002
0368-2048/

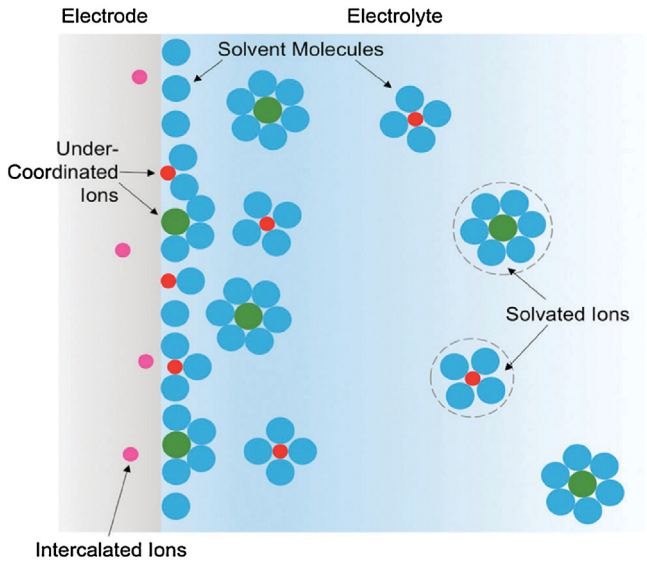

Fig. 1. Schematic illustration of the electrochemical double layer (EDL). Reprinted with permission from [11]. Copyright (2015), Royal Society of Chemistry.

were performed in an *ex-situ* manner, by removing the liquid layer prior to the surface characterization. The lack of *in-situ* characterization tools has been a limiting factor that hinders the experimental investigation on such solid/liquid interface [12], especially those loosely adsorbed species and dynamic processes that only take place with the presence of liquid.

Over the last decade, intense efforts have been devoted to the development of *in-situ*/*operando* characterization techniques which allow the direct observation of the embedded solid/liquid interface with the presence of liquid. Many of the newly developed *in-situ*/*operando* techniques are based on the traditional surface science techniques, but have overcome the conventional vacuum requirements via instrumental innovations. Successful examples include high-pressure STM [20–22], environmental TEM/STEM/EELS [23–27], ambient-pressure XPS [22], and liquid-cell-based soft XAS technique [28–30]. In this review, we will focus on the *in-situ*/*operando* characterization of electrode/electrolyte interfaces using the liquid-cell-based XAS approach. We will present an overview on the *in-situ* sXAS characterization technique and its applications in the studies of electrode/electrolyte interfaces in several electrochemical systems to reveal different aspects of such interfaces, including (i) the adsorption and deposition of electrolyte ions to the electrode surface, (ii) morphological and chemical changes of electrode surfaces under the influence of solution and potentials, and (iii) solvent molecule orientation and its dependence on the electric field. These case studies illustrated the capability of *in-situ*/*operando* sXAS technique, which can be useful for mechanistic investigations of many other energy-related electrochemical systems.

2. Soft x-ray absorption spectroscopy (sXAS) and experimental configuration of liquid-cell-based sXAS

In an x-ray absorption event, an x-ray photon excites a core electron to the unoccupied states in the materials (i.e., the conduction band of a solid materials or the lowest unoccupied molecular orbitals (LUMOs) of a molecule) and creates a hole in the core states [31]. According to Fermi's golden rule, the transition probability of such an excitation event is proportional to the joint density of core-level states and unoccupied states. The element-dependence of core-level energy positions makes XAS element-specific. Meanwhile, because the unoccupied states are greatly affected by the bonding environments of the probed atoms, XAS can also provide information regarding the chemical states of the probed element [32]. The energy range of soft x-rays, typically 100 eV–1500 eV, is suitable to access 1s orbitals of light elements such as C, N, O, F, Na, and Mg, as well as 2p orbitals of 3d transition metals such as Ti, V, Cr, Mn, Fe, Co, Ni, Cu. Many of these elements are involved or even play the key roles in various energy-related systems.

However, the interaction between (soft) x-ray photons and condensed matter such as solids and liquids is so strong that measureable intensity of the transmitted photon flux would require ultra-thin and uniform sample slices, which is unrealistic for most of the materials of interest. Instead of directly recording the transmitted photon flux, the decay process of the core hole created in the XAS event can also be monitored by measuring the emitted electrons or photons following the repopulation of the core hole states [33,34]. In principle, the intensities of these secondary signal are proportional to the absorption intensity and therefore can be used to represent XAS intensity. The secondary electron signal or electron yield (EY) signal can be monitored by measuring the surface drain current (typically called total electron yield or TEY) or by collecting emitted electrons of certain kinetic energies (or within certain energy ranges) using an electron analyzer (called partial electron yield or PEY). With a photon detector or spectrometer, one can record the fluorescence yield (FY) signal. Because the mean free path of x-ray photons is generally much larger than electrons (hundreds of nanometers for soft x-rays *vs* a few nanometers for electrons), FY signal is relatively bulk-sensitive while EY signal is generally more surface-sensitive [35,36]. Within the energy range of soft x-rays, the dominant decay process is the emission of secondary electron (mostly Auger electron) while fluorescence yield is extremely low, typically less than 1% [37].

Conventionally, soft-x-ray-based techniques require vacuum chambers because of strong scattering of photons (and secondary electrons as well) by gas molecules under ambient pressures. The vacuum requirement makes it challenging to directly measure ambient-condition liquids or solid/liquid interfaces using conventional soft x-ray setup. One strategy to overcome the vacuum requirement is to use x-ray transparent membrane to encapsulate liquid samples. With substantial efforts in instrument development, such encapsulation or liquid cell strategy has been successfully used not only in soft x-ray setups but also in various transmission electron microscopy (TEM) instruments [23,27]. Common materials for such x-ray transparent membranes include Si_3N_4, SiO_2, Si and graphene.

Fig. 2(a) showed the schematic design of a flow liquid cell that was developed at the Advanced Light Source (ALS). The Si_3N_4 membrane (typically 100 nm) separates the vacuum environment in the sXAS chamber and the ambient-condition liquid inside the cell. A thin film of the electrode materials of interest, such as 20 nm Au as shown in Fig. 2(a), can be deposited on one side of the Si_3N_4 membrane facing the electrolyte. The incorporation of thin Pt and Ag wires as counter electrode and quasi-reference electrode makes it possible to run electrochemistry inside the cell and perform *in-situ*/*operando* sXAS measurements. Liquid inlet and outlet allows refreshing electrolytes during the experiments. A simpler version of such cell called "static cell" is designed using the same principle but without the liquid inlet/outlet [38,39]. Static cells were first utilized to investigate various bulk liquids system, for instance, water, alcohols, and their mixtures [40–42]. Since electrons cannot pass through the 100 nm membrane, only FY signal was used to characterize the bulk liquids, which provided invaluable information regarding the chemical bonding environment in the bulk liquids. Both static cell and flow cell have been used to study the chemical changes in the bulk electrode under electrochemical conditions, mostly using FY mode [43–46].

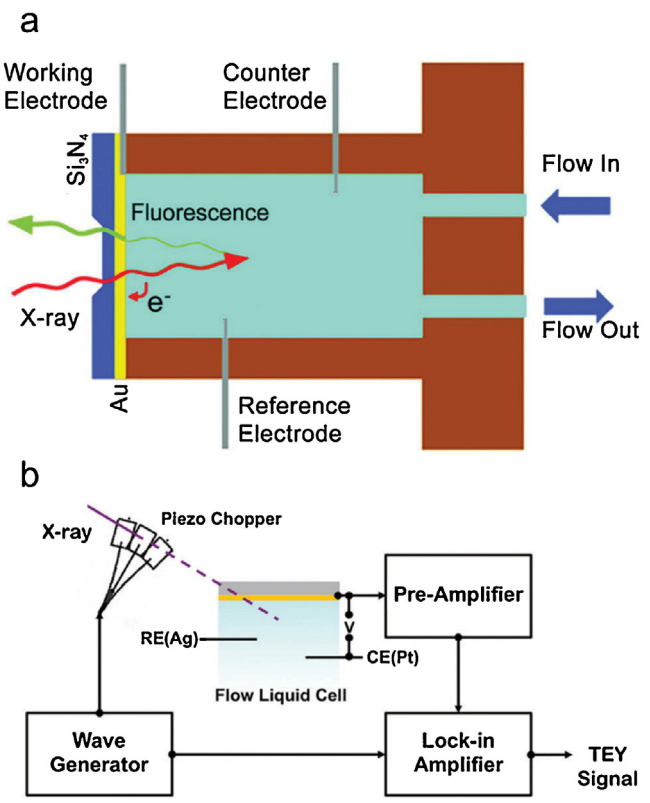

Fig. 2. Experimental configuration of the liquid-cell-based *in-situ/operando* sXAS. (a) Schematic design of the liquid cell for *in-situ/operando* characterization of ambient-condition systems. Reprinted with permission from [47]. Copyright (2014), AAAS. (b) The schematic of x-ray chopper and lock-in system used to extract neat TEY signal in *operando* sXAS measurements. Reprinted with permission from [11]. Copyright (2015), Royal Society of Chemistry.

Recently, using the flow liquid cell, Velasco-Velez et al. have demonstrated the possibility of collecting the secondary electron current generated at the electrode/electrolyte interface through the working electrode [47]. Small mean free path of these secondary electrons, typically a few nm, makes such TEY signal sensitive to the solid/liquid interfaces. Under electrochemical conditions, the dominant ionic current can be separated from the tiny TEY current via a frequency modulation method. As shown in Fig. 2(b), a piezo-actuated chopper was introduced in the beamline to modulate the incoming x-ray at a designed frequency. Intermittent x-ray generates an AC component in the overall current (including both ionic and TEY current), which can then be filtered out using lock-in amplifiers and other necessary electronics. The new development of *in-situ*/*operando* interface-sensitive sXAS provides new opportunities to investigate various solid/liquid interfaces in various important electrochemical systems.

Case study 1: adsorption and deposition of solute species in Mg-ion batteries

Mg-ion batteries have attracted enormous interest because of high theoretical volumetric capacity (3833 $mAhcm^{-3}$) compared to current Li-ion batteries and potentially dendrite-free deposition from the Mg-based electrolyte [48]. One main obstacle for the practical application of Mg batteries is robust electrolyte systems in order to achieve satisfying electrochemical performance and cyclicality. *In-situ/operando* characterization of relevant electrolyte systems can potentially provide invaluable information regarding the reaction mechanism in Mg-ion batteries and help the development and improvement of suitable electrolyte systems.

Using the above-mentioned static liquid cell, Arthur et al. and Benmayza et al. have investigated the electrochemical deposition on a Pt electrode from a Mg-ion electrolyte, i.e., the solution of Mg salt $[Mg_2(\mu\text{-}Cl)_3{\cdot}6(OC_4H_8)]\text{-}(AlCl_4)$ dissolved in tetrahydrofuran (THT) [49,50]. In this experiment, a Pt thin film was evaporated on the Si_3N_4 membrane as the working electrode, while two Pt wires served as counter and reference electrode, respectively. After Mg deposition, Mg K-edge TFY-XAS spectra showed almost identical features as the reference spectrum of Mg metal foil, as shown in Fig. 3(a). After dissolution of the deposited Mg film, the XAS spectrum only exhibited the features related to the Mg salt in the electrolyte, just like the spectrum before any Mg-deposition.

Mg K-edge spectra were also collected while keeping the potentials at −0.1, −0.2, and −0.4 V vs reference electrode, representing pre-deposition, onset of deposition, and post-deposition conditions, as highlighted on the cathodic half-wave in Fig. 3(b). At −0.1 V, a small pre-edge bump appeared in the XAS spectra as shown in Fig. 3(c). The energy position of this new feature resides between the main features of electrodeposited metallic Mg and the Mg salt in the electrolyte. The fact that this pre-edge feature showed up even before the onset potential of Mg deposition indicated that this feature is likely associated with certain intermediate Mg species adsorbed at the electrode/electrolyte interface. This pre-edge feature continued to grow with more negative potentials and eventually red-shifted to the peak position of metallic Mg as bulk deposition of Mg took place. To further unravel the evolution of coordination environment of Mg ion from electrolyte to the electrode surface, the extended x-ray absorption fine structure (EXAFS) at Mg K-edge was also recorded. Fig. 3(d) showed the Fourier-transform intensities of the extended region of XAS spectra *vs* real-space distance. The spectrum of the electrolyte showed a single peak at 1.9 Å with relatively weak resonant structures, indicating the existence of strongly coordinated first shell around Mg ions. A 0.6 Å red shift was observed in the spectrum collected at −0.1 V, which also suggested an intermediate Mg species before the electrodeposition. At more negative potentials, the main peak appeared at 2.9 Å with prominent resonant features, indicative of bulk Mg deposition.

Combining the information from the *in-situ/operando* XAS data and some electrochemical measurements, Benmayza et al. proposed a possible intermediate species during the electrodeposition, i.e., $[M\text{-}MgCl{\cdot}5(OC_4H_8)]^+_{ads}$, where M refers to the substrate, and $[MgCl{\cdot}5(OC_4H_8)]^+$ originates from the dissolution of the Mg dimer. Such intermediate species start to form even before the onset potential of electrodeposition and eventually dissociated and reduced on the electrode surfaces and form bulk metallic Mg.

The ion deposition/dissolution process is one of the most important chemical processes in various metal-ion batteries. The case study on Mg-ion batteries illustrated the capability of such *in-situ/operando* sXAS technique to unravel the reaction mechanism and identify reaction intermediates at the electrode/electrolyte interface during the electrodeposition reaction.

Case study 2: morphological and chemical modification of graphene-based electrode under the influence of electrolytes and potentials

The transport and deposition of ions in the proximity of the electrode surfaces have great impact on the performance of electrochemical devices and can be studied using *in-situ/operando* sXAS techniques, as demonstrated in the case of Mg batteries. What's equally important is the dynamic physicochemical response of the electrode under electrochemical conditions [51]. *In-situ/operando* sXAS can also be used to investigate the surface evolution of electrodes under electrochemical conditions.

Carbon-based materials, such as graphite, graphene, and carbon nanotubes, are widely used as electrodes in various energy storage devices. Electrochemical performances of the devices that contain carbon-based electrodes have been extensively examined but the detailed mechanism especially on the molecular level is

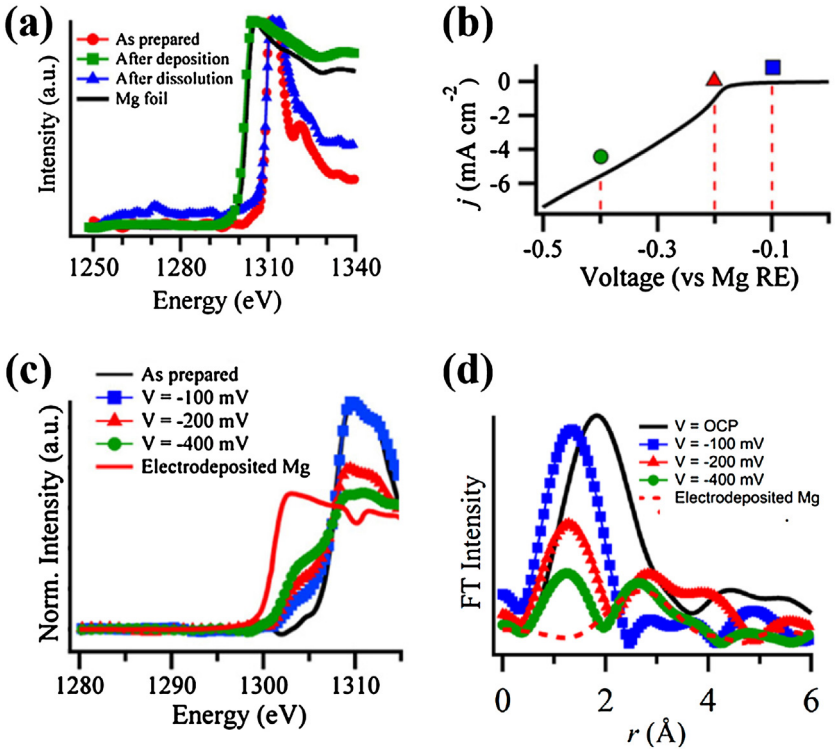

Fig. 3. *In-situ/operando* sXAS characterization on the Mg-ion battery system. (a) Mg K-edge XAS spectra recorded before and after galvanic Mg deposition and dissolution. (b) Cathodic wave for the deposition of Mg from the electrolyte with a green circle, a red triangle, and a blue square highlighting the three potentials where XAS spectra in (c) and (d) were acquired. (c) Near-edge Mg K-edge XAS spectra and (d) Fourier-transformed EXAFS acquired at OCP, −100 mV, −200 mV, and −400 mV, corresponding to conditions of electrolyte only, pre-deposition, onset of deposition, and post-deposition. (a-c) were adapted with permission from [49], Copyright (2012), Elsevier; (d) were adapted with permission [50]. Copyright (2013), ACS publications. (For interpretation of the references to colour in this figure legend, the reader is referred to the web version of this article.)

not well understood, partly because of the lack of *in-situ/operando* characterization techniques. Using the liquid cell described earlier, Velasco-Velez et al. investigated the structural and chemical modifications on a single layer graphene (SGL) as a model electrode surface under electrochemistry-relevant conditions [52]. Because SGL only has one atomic layer, both TFY and TEY XAS spectra provide essentially the same information.

The SGL grown via chemical vapor deposition (CVD) methods was transferred onto the Si_3N_4 membrane as the working electrode [53]. Before being put in contact with aqueous solution, as-transferred graphene electrode was characterized in vacuum by sXAS. C K-edge XAS spectrum of as-prepared graphene electrode, as shown in Fig. 4(a), is similar to that of highly ordered pyrolytic graphite (HOPG), exhibiting two dominant features: The sharp peak at 285.5 eV corresponds to the 1s-π^* transition, while the peak at 291.5 eV is related to the transition to σ^* states [54]. Once the SGL electrode was put in contact with the 2 mM NaCl solution, its C K-edge spectra showed substantial broadening of both π^* and σ^* peaks. Meanwhile, two new features between the π^* and σ^* peaks, labeled as C and D in Fig. 4(b), appeared, which are possibly related to C—OH and —COOH species [36]. The spectral changes indicated that even before applying any electrochemical potentials, chemical modification already took place on the SGL electrode. The spectral evolution as a function of numbers of cyclic voltammetry (CV) cycles (between −1 V and 1 V, two-electrode configuration) shown in Fig. 4(b) exhibit further modifications on the SGL electrode and many different carbon species may be involved as suggested by the authors. The formation of various carbon species on the graphene surface suggested opening of carbon rings and adsorption or addition of —H, —O, or —OH groups. More aggressive electrochemical conditions make the SGL sheet even more defective, as suggested by both *in-situ* XAS and *ex-situ* AFM and Raman spectroscopy measurements.

In-situ sXAS also revealed that being in contact with NaCl solution induced not only chemical modifications but also morphological changes to the defective SGL. From the angle-dependent C K-edge XAS spectra of partially oxidized graphene (POG), POG in contact with NaCl solution in static cell, and POG in contact with water for 7 days, Velasco-Velez et al. were able to extract the dichroic ratio (DR) of three different graphene samples and make quantitative comparison of the surface corrugation between these graphene samples [52]. A perfectly flat graphene would have a DR value of −1 [55]. DR value of the starting materials, i.e., the CVD grown graphene on Cu substrate, is −0.88. DR value decreased to −0.7 once the graphene was transferred onto the Si_3N_4 membrane. This value went down to −0.5 once the single-layer POG was in contact with NaCl solution and further down to −0.4 after the graphene was exposed to aqueous solution for 7 days, indicating further corrugation of the graphene sheets.

Bagge-Hansen et al. used the similar *in-situ* setup to investigate the structural and chemical modification on a more practical graphene-based electrode, i.e. 3D nanographene (3D-NG) electrode, in a supercapacitor system [56]. All spectra were recorded in TFY mode. Fig. 5(a)–(c) showed the C K-edge XAS spectra of the 3D-NG electrode in 1 M NaCl solution under different constant bias between −1 V and 1 V *vs* reference electrode. Under negative potentials up to −1 V, the spectra of 3D-NG electrode exhibited no obvious difference compared to the spectra collected under open circuit potential (OCP), while substantial changes were observed in the C K-edge spectra under positive potentials. Self-consistent spectra fitting revealed two resonance features (labeled as α and β in Fig. 5) with the most substantial changes under positive poten-

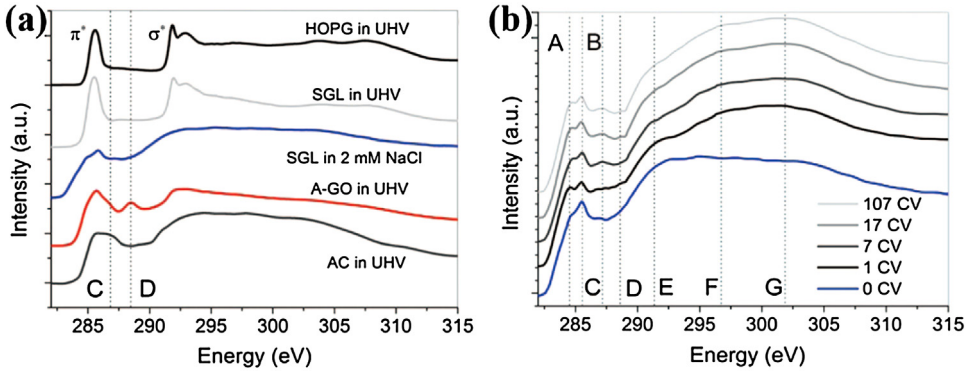

Fig. 4. *In-situ/operando* sXAS characterization of single layer graphene (SGL) electrode. (a) C K-edge TEY-XAS spectra of HOPG in UHV, SGL in UHV, graphene in contact with 2 mM NaCl, acid-treated graphene oxide A-GO, and amorphous carbon. (b) C K-edge TEY-XAS spectra of SGL electrode in contacting with NaCl electrolyte after different numbers of CV cycles. Reprinted with permission from [53], Copyright (2013), The Electrochemical Society.

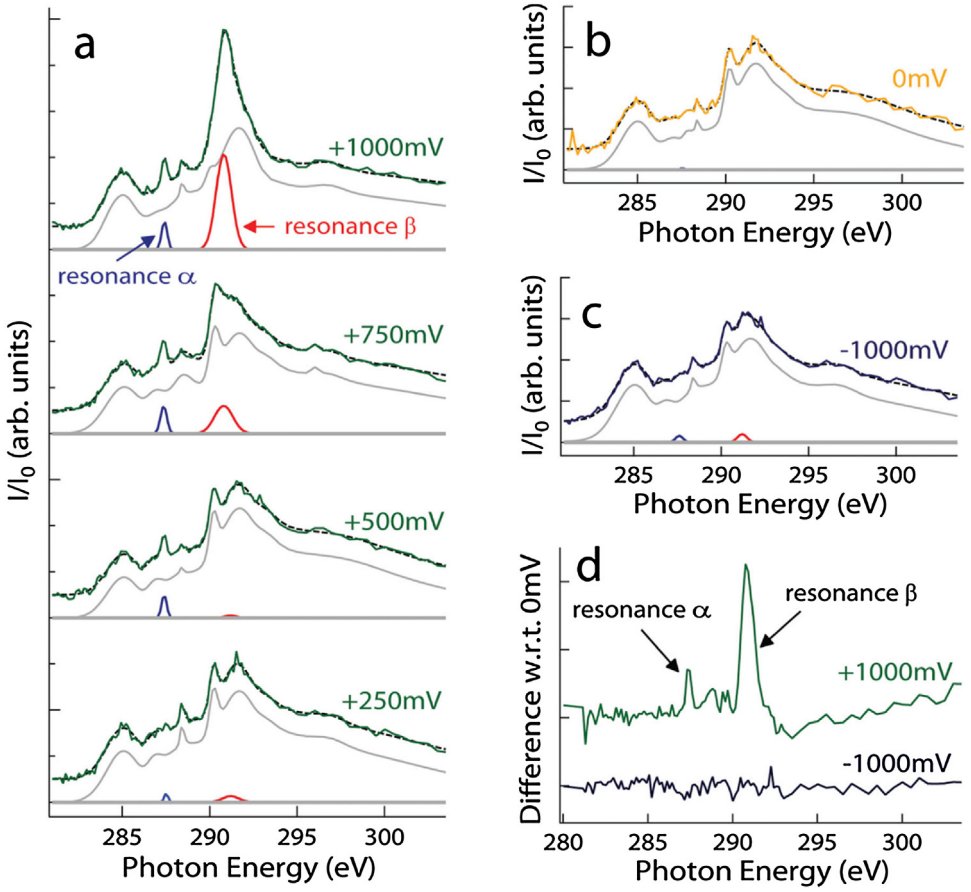

Fig. 5. *Operando* sXAS investigation of 3D-NG electrode in supercapacitors. C K-edge TFY-XAS spectra of 3D-NG electrode in contact with 1 M NaCl solution under: a) constant external potentials between +250 and +1000 mV (green), b) 0 mV (orange), and c) −1000 mV (dark blue). (d) Intensity difference between sXAS spectra at 100 mV and 0 mV, −1000 mV and 0 mV. Reprinted with permission from [56], Copyright (2015), John Wiley and Sons. (For interpretation of the references to colour in this figure legend, the reader is referred to the web version of this article.)

tials, located at 287.3 eV and 291 eV, respectively [36,56]. These two resonance features were also observable in the intensity difference between the spectra collected at 0 V and +1 V, as shown in Fig. 5(d). The origin of these two resonances has been further investigated via theoretical simulations. Simulation results suggested that the peak α is related to the σ* resonances of C—OH despite of high concentration of Cl^- in the electrolyte; whereas intensity change in peak β is likely due to the modification on C—C bond geometry induced by out-of-plane distortion and consequent surface strain upon massive OH^- (covalent) adsorption on the graphene surfaces. These results are also partly in line with the reports on the *in-situ* characterizations SGL by Velasco-Velez et al.

These observations illustrated the complexity in the changes of the electrode materials during electrochemical processes. Electrode materials, especially the surface of the electrode, can undergo a series of chemical, electronic, morphological changes under different electrochemical conditions, which can be captured by *in-situ*/operando sXAS characterizations.

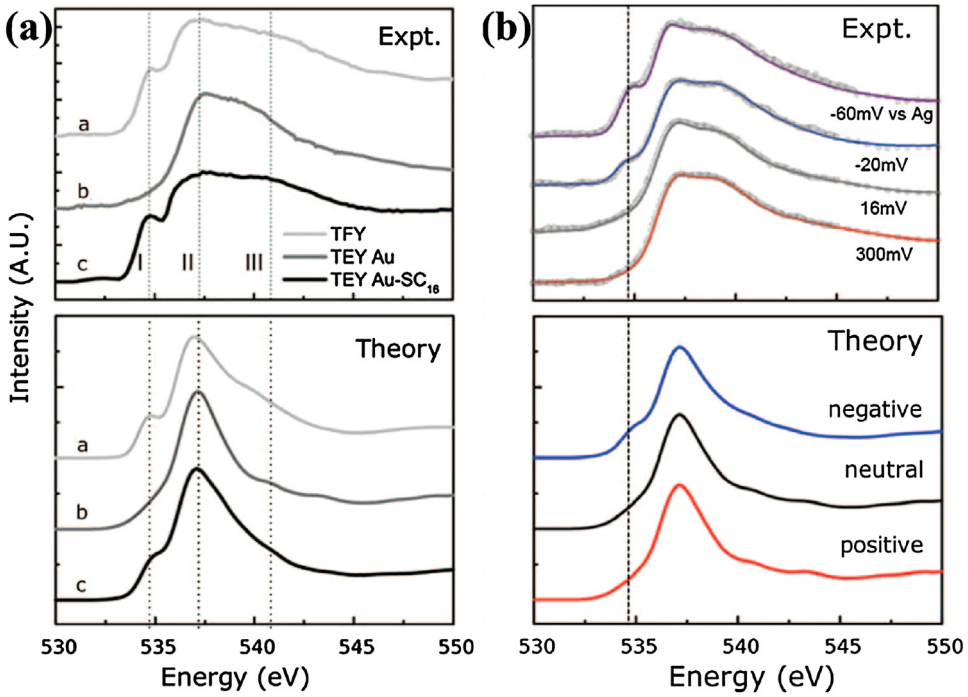

Fig. 6. *In-situ/operando* sXAS characterization of interfacial water on Au surface. (a) Experimental and theoretical O K-edge XAS spectra collected at the water/Au interface under OCP condition. (b) Experimental and theoretical O K-edge XAS spectra collected on the water/Au interface under negative, neutral, and positive potentials. Reprinted with permission from [47], Copyright (2014), AAAS.

Case study 3: potential-dependent orientation of solvent molecules at Au/water interface

Solvent molecules are equally important in various electrochemical systems, but are often overlooked at the solid/liquid interface, especially when the solvent molecules don't directly participate in the reactions. However, the properties and behaviors of the solvent molecules at the solid/liquid interfaces can greatly influence the ion solvation, mass transport, hydrogen bond network, and potential drop profile in the electrical double layer.

Using the TEY-based *operando* XAS, Velasco-Velez et al. studied the interfacial water molecules on gold electrode [47]. A 20nm-thick Au film, as the working electrode, was evaporated on the Si_3N_4 membrane, in contact with 10 μM NaCl solution. In water, the mean free path of electrons around 500 eV (close to the O1 s absorption edge) is ~1 nm, which corresponds to just two to three water layers close to the surface of the Au electrode. Fig. 6(a) showed the O K-edge TEY and TFY XAS spectra collected when the Au thin film electrode was in contact with low concentration NaCl solution. Prominent pre-edge feature around 535 eV could be observed in TFY spectra, which is associated with the dangling hydrogen bonds [57]. Such pre-edge feature was substantially weaker in the TEY spectra. Control experiments on C_{16}-thiol covered Au electrode proved that such suppression of pre-peak feature is a direct consequence of physical contact between water and Au surface, because once the water molecules was spatially separated from the Au surface by the self-assembled thiol layer, the pre-peak feature reappeared in the TEY XAS spectrum. First-principle simulations revealed that the suppression of the pre-peak feature is originated from the delocalization of the LUMO orbitals of interfacial water molecules into the surrounding Au atoms, which effectively reduces the spatial overlap of the core-hole states and the LUMO orbitals and thereby decreases relevant transition probability and suppresses the pre-peak feature. Furthermore, the electronic coupling effect between interfacial water and Au substrate decays rapidly with Au-water distance and the intensity reduction of the pre-peak feature for the second layer water molecules are ~30% of that of the first layer. The fact that the pre-peak feature is greatly suppressed in the TEY signal compared to TFY signal hinted that TEY signal in this case is highly interface sensitive [11].

With the x-ray modulation and lock-in system, Velasco-Velez et al. were also able to collect such interface-sensitive TEY XAS spectra under different potentials, as shown in Fig. 6(b). Under negative bias, water molecules are expected to point more H atoms towards to the Au surface, generating more dangling hydrogen bonds. Although the pre-peak feature is suppressed in the XAS spectrum of all the interfacial water molecules, but the increase in total concentration of dangling hydrogen bonds at the Au/water interface made the pre-peak feature reappear in the TEY XAS spectrum. On the contrary, under positive bias, the pre-peak feature is still suppressed, because interfacial water molecules point more O atoms to the positively charged Au surface, which provide more opportunities for the H atoms of these interfacial water molecules to form hydrogen bonds with surrounding water molecules.

This *in-situ*/*operando* XAS study on interfacial water on Au demonstrated the interface sensitivity of such TEY-based XAS methods. It also illustrated the complexities in the behavior of polar solvent molecules at the electrode/electrolyte interface under electrochemical conditions, such as electronic coupling with the substrates and potential-dependent orientation. These complex behaviors of solvent molecules must play certain roles in the overall interface processes, and such *in-situ*/*operando* XAS techniques can be a useful tool to unravel some of these mysteries at the electrode/electrolyte interfaces.

3. Conclusion and final remarks

The interface between solid electrode and liquid electrolyte is where most important chemical processes take place in every electrochemical system. Despite its importance, such solid/liquid interface is still not well understood, especially at the molecular or atomic level. Therefore, advanced *in-situ*/*operando* characterization techniques are desired to better understand the interfacial

complexities. The element- and chemical-specific sXAS technique is a useful characterization tool and the development of liquid cells allows the *in-situ/operando* sXAS characterization on ambient-condition systems. More importantly, TEY-XAS can potentially provide surface-/interface-sensitive information in various electrochemical systems. Here we reviewed several recent examples using such *in-situ/operando* sXAS methods to investigate electrodeposition of Mg in Mg-ion batteries, chemical and structural modification on graphene-based electrode in supercapacitors, and potential-dependent orientation of interfacial water on Au surfaces. All these recent examples demonstrated the capability of *in-situ/operando* sXAS techniques in the investigation of different aspects of the solid/liquid interfaces. Together with other newly developed *in-situ/operando* techniques, the liquid-cell-based sXAS technique provides exciting new opportunities for the scientists to take a closer look at the solid/liquid interfaces.

Finally, the construction of new synchrotron facilities and upgrade on the existing ones around the globe are making such synchrotron-based techniques more accessible to the researcher community. Newer-generation synchrotrons can also provide higher brilliance x-rays, which facilitates more efficient data collection as well as the development of new characterization techniques that was unrealistic with low photon flux. On the other hand, high-energy probes such as x-rays can induce severe beam damage to the samples or reaction systems of interest, which may lead to side reactions and inaccurate experiment data. Thus, control experiments are necessary to rule out beam-induced effect and make accurate data interpretation. To avoid or minimize the impact of beam-induced effect, precautions need to be taken, for instance, reducing the x-ray flux, defocusing the x-ray beam, avoiding unnecessary x-ray illumination during measurement and so on.

Acknowledgements

The Advanced Light Source is supported by the Director, Office of Science, Office of Basic Energy Sciences, of the U.S. Department of Energy under Contract No. DE-AC02-05CH11231.

References

[1] M. Kapilashrami, Y. Zhang, Y.-S. Liu, A. Hagfeldt, J. Guo, Probing the optical property and electronic structure of TiO2 nanomaterials for renewable energy applications, Chem. Rev. 114 (2014) 9662–9707.
[2] M.G. Walter, E.L. Warren, J.R. McKone, S.W. Boettcher, Q. Mi, E.A. Santori, N.S. Lewis, Solar water splitting cells, Chem. Rev. 110 (2010) 6446–6473.
[3] M. Gratzel, Photoelectrochemical cells, Nature 414 (2001) 338–344.
[4] B.C.H. Steele, A. Heinzel, Materials for fuel-cell technologies, Nature 414 (2001) 345–352.
[5] S. Min-Kyu, J.C. Elton, Z. Yuegang, Lithium/sulfur batteries with high specific energy: old challenges and new opportunities, Nanoscale 5 (2013).
[6] T. Gao, M. Noked, A.J. Pearse, E. Gillette, X. Fan, Y. Zhu, C. Luo, L. Suo, M.A. Schroeder, K. Xu, S.B. Lee, G.W. Rubloff, C. Wang, Enhancing the reversibility of Mg/S battery chemistry through Li+ mediation, J. Am. Chem. Soc. 137 (2015) 12388–12393.
[7] J.B. Goodenough, K.-S. Park, The Li-ion rechargeable battery: a perspective, J. Am. Chem. Soc. 135 (2013) 1167–1176.
[8] A.J. Bard, L.R. Faulkner, Electrochemical Methods: Fundamentals and Applications, Wiley, 2000.
[9] R. Parsons, The electrical double layer: recent experimental and theoretical developments, Chem. Rev. 90 (1990) 813–826.
[10] P. Attard, Electrolytes and the Electric Double Layer, Advances in Chemical Physics, John Wiley & Sons, Inc., 2007, pp. 1–159.
[11] C.H. Wu, R.S. Weatherup, M.B. Salmeron, Probing electrode/electrolyte interfaces in situ by X-ray spectroscopies: old methods new tricks, Phys. Chem. Chem. Phys. 17 (2015) 30229–30239.
[12] M. Fleischmann, B.W. Mao, In-situ X-ray diffraction studies of Pt electrode/solution interfaces, J. Electroanal. Chem. Interfacial Electrochem. 229 (1987) 125–139.
[13] C. Stuhlmann, Z. Park, C. Bach, K. Wandelt, An ex-situ study of Cd underpotential deposition on Cu(111), Electrochim. Acta 44 (1998) 993–998.
[14] M.V. Lebedev, W. Calvet, T. Mayer, W. Jaegermann, Photoelectrochemical processes at n-GaAs(100)/aqueous HCl electrolyte interface: a synchrotron photoemission spectroscopy study of emersed electrodes, J. Phys. Chem. C 118 (2014) 12774–12781.
[15] D.M. Seo, C.C. Nguyen, B.T. Young, D.R. Heskett, J.C. Woicik, B.L. Lucht, Characterizing solid electrolyte interphase on Sn anode in lithium ion battery, J. Electrochem. Soc. 162 (2015) A7091–A7095.
[16] F. Lin, I.M. Markus, D. Nordlund, T.-C. Weng, M.D. Asta, H.L. Xin, M.M. Doeff, Surface reconstruction and chemical evolution of stoichiometric layered cathode materials for lithium-ion batteries, Nat. Commun. 5 (2014) 3529.
[17] L. Qinghao, Q. Ruimin, L.A. Wray, C. Jun, Z. Zengqing, C. Yanxue, Y. Shishen, P. Feng, H. Zahid, Y. Wanli, Quantitative probe of the transition metal redox in battery electrodes through soft x-ray absorption spectroscopy, J. Phys. D: Appl. Phys. 49 (2016) 413003.
[18] J. Cerdá, A. Michaelides, M.L. Bocquet, P.J. Feibelman, T. Mitsui, M. Rose, E. Fomin, M. Salmeron, Novel water overlayer growth on Pd(111) characterized with scanning tunneling microscopy and density functional theory, Phys. Rev. Lett. 93 (2004) 116101.
[19] Y. Li, F. El Gabaly, T.R. Ferguson, R.B. Smith, N.C. Bartelt, J.D. Sugar, K.R. Fenton, D.A. Cogswell, A.L.D. Kilcoyne, T. Tyliszczak, M.Z. Bazant, W.C. Chueh, Current-induced transition from particle-by-particle to concurrent intercalation in phase-separating battery electrodes, Nat. Mater. 13 (2014) 1149–1156.
[20] K. Voïtchovsky, Anharmonicity, solvation forces, and resolution in atomic force microscopy at the solid-liquid interface, Phys. Rev. E 88 (2013) 022407.
[21] B. Eren, Z. Liu, D. Stacchiola, G.A. Somorjai, M. Salmeron, Structural changes of cu(110) and Cu(110)-(2 × 1)-O surfaces under carbon monoxide in the torr pressure range studied with scanning tunneling microscopy and infrared reflection absorption spectroscopy, J. Phys. Chem. C 120 (2016) 8227–8231.
[22] B. Eren, R.S. Weatherup, N. Liakakos, G.A. Somorjai, M. Salmeron, Dissociative carbon dioxide adsorption and morphological changes on cu(100) and Cu(111) at ambient pressures, J. Am. Chem. Soc. 138 (2016) 8207–8211.
[23] H. Zheng, R.K. Smith, Y.-w. Jun, C. Kisielowski, U. Dahmen, A.P. Alivisatos, Observation of single colloidal platinum nanocrystal growth trajectories, Science 324 (2009) 1309–1312.
[24] H. Zheng, Y.S. Meng, Y. Zhu, Frontiers of in situ electron microscopy, MRS Bull. 40 (2015) 12–18.
[25] H.-G. Liao, L. Cui, S. Whitelam, H. Zheng, Real-time imaging of Pt_3Fe nanorod growth in solution, Science 336 (2012) 1011–1014.
[26] H.-G. Liao, D. Zherebetskyy, H. Xin, C. Czarnik, P. Ercius, H. Elmlund, M. Pan, L.-W. Wang, H. Zheng, Facet development during platinum nanocube growth, Science 345 (2014) 916–919.
[27] Z. Zeng, W.-I. Liang, H.-G. Liao, H.L. Xin, Y.-H. Chu, H. Zheng, Visualization of electrode–electrolyte interfaces in LiPF6/EC/DEC electrolyte for lithium ion batteries via in situ TEM, Nano Lett. 14 (2014) 1745–1750.
[28] G.G. Long, J. Kruger, D.R. Black, M. Kuriyama, EXAFS study of the passive film on iron, J. Electrochem. Soc. 130 (1983) 240–242.
[29] A.J. Davenport, H.S. Isaacs, G.S. Frankel, A.G. Schrott, C.V. Jahnes, M.A. Russak, In situ X-ray absorption study of chromium valency changes in passive oxides on sputtered AlCr thin films under electrochemical control, J. Electrochem. Soc. 138 (1991) 337–338.
[30] G.S. Frankel, A.J. Davenport, H.S. Isaacs, A.G. Schrott, C.V. Jahnes, M.A. Russak, X-ray absorption study of electrochemically grown oxide films on Al-Cr sputtered alloys: I. Ex situ studies, J. Electrochem. Soc. 139 (1992) 1812–1820.
[31] F. de Groot, High-resolution X-ray emission and X-ray absorption spectroscopy, Chem. Rev. 101 (2001) 1779–1808.
[32] J. Guo, Soft X-Ray Absorption and Emission Spectroscopy in the Studies of Nanomaterials, X-Rays in Nanoscience, Wiley-VCH Verlag GmbH & Co. KGaA, 2010, pp. 211–254.
[33] M. Giorgetti, A review on the structural studies of batteries and host materials by X-ray absorption spectroscopy, ISRN Mater. Sci. 2013 (2013) 22.
[34] B.H. Frazer, B. Gilbert, B.R. Sonderegger, G. De Stasio, The probing depth of total electron yield in the sub-keV range: TEY-XAS and X-PEEM, Surf. Sci. 537 (2003) 161–167.
[35] Y. Ye, A. Kawase, M.-K. Song, B. Feng, Y.-S. Liu, M.A. Marcus, J. Feng, H. Fang, E.J. Cairns, J. Zhu, J. Guo, X-ray absorption spectroscopic characterization of the synthesis process: revealing the interactions in cetyltrimethylammonium bromide-modified sulfur–graphene oxide nanocomposites, J. Phys. Chem. C 120 (2016) 10111–10117.
[36] Y. Ye, A. Kawase, M.-K. Song, B. Feng, Y.-S. Liu, M. Marcus, J. Feng, E. Cairns, J. Guo, J. Zhu, X-ray absorption spectroscopy characterization of a Li/S cell, Nanomaterials 6 (2016) 14.
[37] M.O. Krause, Atomic radiative and radiationless yields for K and L shells, J. Phys. Chem. Ref. Data 8 (1979) 307–327.
[38] Y.-S. Liu, P.-A. Glans, C.-H. Chuang, M. Kapilashrami, J. Guo, Perspectives of in situ/operando resonant inelastic X-ray scattering in catalytic energy materials science, J. Electron Spectrosc. Relat. Phenom. 200 (2015) 282–292.
[39] H. Zhang, W.-C. Wang, P.-A. Glans, Y.-S. Liu, M. Kapilashrami, J.-L. Chen, C. Chang, M. Salmeron, C. Escudero, E. Pach, A. Tuxen, M. Chintapalli, S. Carenco, X. Sun, J. Guo, Developing soft X-ray spectroscopy for in situ characterization of nanocatalysts in catalytic reactions, J. Electron Spectrosc. Relat. Phenom. 197 (2014) 118–123.
[40] J.H. Guo, Y. Luo, A. Augustsson, J.E. Rubensson, C. Såthe, H. Ågren, H. Siegbahn, J. Nordgren, X-ray emission spectroscopy of hydrogen bonding and electronic structure of liquid water, Phys. Rev. Lett. 89 (2002) 137402.
[41] A. Nilsson, D. Nordlund, I. Waluyo, N. Huang, H. Ogasawara, S. Kaya, U. Bergmann, L.Å. Näslund, H. Öström, P. Wernet, K.J. Andersson, T. Schiros, L.G.M. Pettersson, X-ray absorption spectroscopy and X-ray Raman scattering

of water and ice; an experimental view, J. Electron Spectrosc. Relat. Phenom. 177 (2010) 99–129.
[42] J.H. Guo, Y. Luo, A. Augustsson, S. Kashtanov, J.E. Rubensson, D.K. Shuh, H. Ågren, J. Nordgren, Molecular structure of alcohol-water mixtures, Phys. Rev. Lett. 91 (2003) 157401.
[43] S. Carenco, A. Tuxen, M. Chintapalli, E. Pach, C. Escudero, T.D. Ewers, P. Jiang, F. Borondics, G. Thornton, A.P. Alivisatos, H. Bluhm, J. Guo, M. Salmeron, Dealloying of cobalt from CuCo nanoparticles under syngas exposure, J. Phys. Chem. C 117 (2013) 6259–6266.
[44] A. Tuxen, S. Carenco, M. Chintapalli, C.-H. Chuang, C. Escudero, E. Pach, P. Jiang, F. Borondics, B. Beberwyck, A.P. Alivisatos, G. Thornton, W.-F. Pong, J. Guo, R. Perez, F. Besenbacher, M. Salmeron, Size-dependent dissociation of carbon monoxide on cobalt nanoparticles, J. Am. Chem. Soc. 135 (2013) 2273–2278.
[45] P. Jiang, D. Prendergast, F. Borondics, S. Porsgaard, L. Giovanetti, E. Pach, J. Newberg, H. Bluhm, F. Besenbacher, M. Salmeron, Experimental and theoretical investigation of the electronic structure of Cu2O and CuO thin films on Cu(110) using x-ray photoelectron and absorption spectroscopy, J. Chem. Phys. 138 (2013) 024704.
[46] C. Escudero, P. Jiang, E. Pach, F. Borondics, M.W. West, A. Tuxen, M. Chintapalli, S. Carenco, J. Guo, M. Salmeron, A reaction cell with sample laser heating for in situ soft X-ray absorption spectroscopy studies under environmental conditions, J. Synchrotron Radiat. 20 (2013) 504–508.
[47] J.-J. Velasco-Velez, C.H. Wu, T.A. Pascal, L.F. Wan, J. Guo, D. Prendergast, M. Salmeron, The structure of interfacial water on gold electrodes studied by x-ray absorption spectroscopy, Science 346 (2014) 831–834.
[48] R. Mohtadi, F. Mizuno, Magnesium batteries: current state of the art, issues and future perspectives, Beilstein J. Nanotechnol. 5 (2014) 1291–1311.
[49] T.S. Arthur, P.-A. Glans, M. Matsui, R. Zhang, B. Ma, J. Guo, Mg deposition observed by in situ electrochemical Mg K-edge X-ray absorption spectroscopy, Electrochem. Commun. 24 (2012) 43–46.
[50] A. Benmayza, M. Ramanathan, T.S. Arthur, M. Matsui, F. Mizuno, J. Guo, P.-A. Glans, J. Prakash, Effect of electrolytic properties of a magnesium organohaloaluminate electrolyte on magnesium deposition, J. Phys. Chem. C 117 (2013) 26881–26888.
[51] I. Heller, J. Kong, K.A. Williams, C. Dekker, S.G. Lemay, Electrochemistry at single-walled carbon nanotubes: the role of band structure and quantum capacitance, J. Am. Chem. Soc. 128 (2006) 7353–7359.
[52] J.J. Velasco-Velez, C.H. Wu, B.Y. Wang, Y. Sun, Y. Zhang, J.H. Guo, M. Salmeron, Polarized X-ray absorption spectroscopy observation of electronic and structural changes of chemical vapor deposition graphene in contact with water, J. Phys. Chem. C 118 (2014) 25456–25459.
[53] J.J. Velasco-Velez, C.-H. Chuang, H.-L. Han, I. Martin-Fernandez, C. Martinez, W.-F. Pong, Y.-R. Shen, F. Wang, Y. Zhang, J. Guo, M. Salmeron, In-situ XAS investigation of the effect of electrochemical reactions on the structure of graphene in aqueous electrolytes, J. Electrochem. Soc. 160 (2013) C445–C450.
[54] R.P. Gandhiraman, D. Nordlund, C. Javier, J.E. Koehne, B. Chen, M. Meyyappan, X-ray absorption study of graphene oxide and transition metal oxide nanocomposites, J. Phys. Chem. C 118 (2014) 18706–18712.
[55] V. Lee, C. Park, C. Jaye, D.A. Fischer, Q. Yu, W. Wu, Z. Liu, J. Bao, S.-S. Pei, C. Smith, P. Lysaght, S. Banerjee, Substrate hybridization and rippling of graphene evidenced by near-edge X-ray absorption fine structure spectroscopy, J. Phys. Chem Lett. 1 (2010) 1247–1253.
[56] M. Bagge-Hansen, B.C. Wood, T. Ogitsu, T.M. Willey, I.C. Tran, A. Wittstock, M.M. Biener, M.D. Merrill, M.A. Worsley, M. Otani, C.-H. Chuang, D. Prendergast, J. Guo, T.F. Baumann, T. van Buuren, J. Biener, J.R.I. Lee, Potential-induced electronic structure changes in supercapacitor electrodes observed by in operando soft X-ray spectroscopy, Adv. Mater. 27 (2015) 1512–1518.
[57] A. Nilsson, L.G.M. Pettersson, Chemical bonding on surfaces probed by X-ray emission spectroscopy and density functional theory, Surf. Sci. Rep. 55 (2004) 49–167.